Skin Research and Technology 2002; 8: 118–124
Printed in Denmark. All rights reserved

Skin Research and Technology
ISSN 0909-752X

Anatomy and physiology of subcutaneous adipose tissue by in vivo magnetic resonance imaging and spectroscopy: Relationships with sex and presence of cellulite

B. Querleux, C. Cornillon, O. Jolivet* and J. Bittoun*
*L'Oréal—Advanced research laboratories, Aulnay-sous-bois, France and *CIERM—ESA CNRS 8081, Le Kremlin-Bicêtre, France*

Background: Little is still known concerning subcutaneous adipose tissue and cellulite, and controversial questions are still under discussion.
Aims: Magnetic resonance imaging and spectroscopy were used to address two unresolved questions relating to the anatomy and physiology of subcutaneous adipose tissue.
Methods: Using high spatial resolution magnetic resonance imaging we characterized the topography of the dermo-hypodermal junction, and the three-dimensional architecture of the subcutaneous fibrous septae. Using proton spectroscopy, we measured water and lipid fractions within a fat lobule, and T_1 and T_2 values of the detected compounds. All these data were analysed according to sex and presence of cellulite.
Results: MR imaging quantified deeper indentations of adipose tissue into the dermis, and evidenced for the first time a great increase in the thickness of the inner fat layer in women with cellulite. Moreover, 3D reconstruction of the fibrous septae network showed a higher percentage of septae in a direction perpendicular to the skin surface in women with cellulite; but our study also depicted the tortuous aspect of this network. MR proton spectroscopy could not show any differences related to sex or presence of cellulite concerning T_1 and T_2 relaxation times of the detected compounds within a fat lobule, neither the unsaturated lipid fraction, the saturated lipid fraction, nor the water fraction.
Conclusions: Magnetic resonance imaging showed that the 3D architecture of fibrous septae couldn't be modelled simply as perpendicular planes for women and tilted planes at 45° for men. MR spectroscopy did not confirm the hypothesis of increased water content in the adipose tissue of women with cellulite as suggested by others, except if such water would be located in the connective septae.

Key words: cellulite – Hypodermis – magnetic resonance imaging – magnetic resonance spectroscopy

Accepted for publication 14 January 2001

The traditional view of subcutaneous adipose tissue relates to its functions of mechanical support and thermal insulation. Recent times have seen a growing interest in the role of adipose tissue distribution and composition in relation to health and disease (1, 2).

Studies on the physiology and anatomy of adipose tissue usually follow two approaches, namely *in vitro* studies of isolated adipocyte or alternatively *in vivo* studies with non-invasive or minimally-invasive functional methods (3–5).

Magnetic resonance (MR) imaging is recognized as a reliable technique for measuring adipose volume according to body site (6, 7), and for differentiating visceral adipose tissue from subcutaneous adipose tissue (8, 9). Beyond the medical interest in characterizing diseased adipose tissue (10–12), MR imaging has proved useful in advancing knowledge in nutrition science (6, 13), in plastic surgery (14), and in cosmetology (15).

Preliminary studies performed with MR spectroscopy had already evidenced some new information about lipid composition in normal (16–20), and diseased adipose tissues (21, 22).

The current concept of the anatomy of adipose tissue derives from the histologic studies of Nürnberger, and Müller (23), who analysed adipose samples of normal men, normal women, and women with cellulite. They reported deep adipose indentations into the dermis in women, but not in

men. They also described modifications of the architecture of the fibrous septae, mainly orientated perpendicular to the skin surface in women and with a criss-cross pattern for men (23). Micro-anatomical description of cellulite was recently critically revisited by Pierard et al. (24). Using *in vivo* high frequency ultrasound imaging, our group (25), and others (26, 27), had confirmed a more undulated dermo-hypodermal interface in women with cellulite. Up till now, there has been no *in vivo* imaging method for visualizing the 3D architecture of the fibrous septae network. Adipose physiology of cellulite has been suggested to be related to lymphovascular disorders (28), but to our knowledge this has not been confirmed by others (27, 29).

In the present study we utilized MR imaging and spectroscopy to clarify these controversial issues concerning the anatomy and physiology of adipose tissue according to sex and presence of cellulite.

Materials and Methods

Subjects

Sixty-seven healthy volunteers participated in the study, which was approved by the hospital ethics committee. The subjects were recruited by a medical expert according to the following main inclusion criteria: age range: 18–45 years, body mass index (BMI): 17–27, constant weight during last year, women with a regular menstrual cycle, and between 0 and 10 days post menstruation at the date of the experiment.

The study site was the upper dorsal thigh. This site, was given privilege to ensure a close contact with the add-on device, i.e. lowering undesired motion artifacts during MR acquisition. The volunteers were divided into three groups by an experienced medical doctor: women with no visible cellulite even after compression at the study site ($n = 21$, age $= 23.5 \pm 3.4$, BMI $= 18.04 \pm 0.65$), women with a clear visible cellulite with and without compression ($n = 23$, age $= 33.6 \pm 8.1$, BMI $= 25.78 \pm 1.42$), and normal men ($n = 23$, age $= 33.1 \pm 6.6$, BMI $= 23.1 \pm 1.43$).

Materials

High resolution MR imaging and spectroscopy were performed on a 1.5 T whole-body MR system (*General Electric, Milwaukee, USA*) equipped with a home-built add-on device comprising a high-intensity surface gradient coil and a small surface radiofrequency coil allowing spatial resolution in the antero-posterior direction of 70 μm (30).

Imaging protocol

Two-dimensional (2D) axial images (Spin echo sequence, repetition time (T_R) = 500 ms, echo time (T_E) = 17 ms, field-of-view (FOV) = 240 × 240 mm^2 (Fig. 1a), and 18 × 50 mm^2 (Fig. 1b), slice thickness = 3 mm, acquisition time (T_{acq}) = 2 min 20 s) were first acquired from which the thickness of subcutaneous adipose tissue was measured. On images with an in-depth resolution of 70 μm, the Camper's fascia was clearly defined and allowed us to differentiate superficial adipose layer from deep adipose layer. A series of 60 axial images was then acquired (3D gradient echo sequence, $T_R = 100$ ms, $T_E = 11$ ms, flip angle 40°, FOV = 18 × 50 mm^2, slice thickness = 0.5 mm, $T_{acq} = 12$ min). With such thin slices (Fig. 1c), the 3D architecture of fibrous network could be analysed within a volume of 20 × 20 × 20 mm^3.

Spectroscopy protocol

A series of three contiguous axial images (voxel size = 70 × 390 × 3000 μm^3) was first obtained

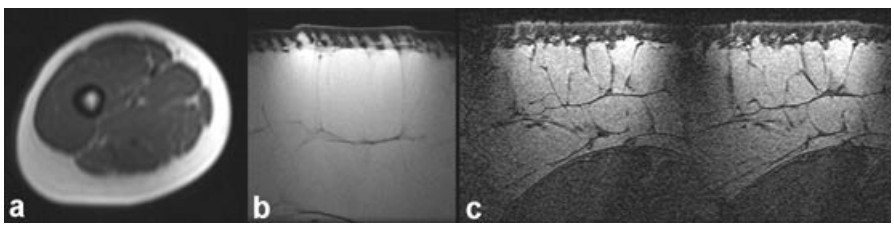

Fig. 1. Magnetic Resonance images of adipose tissue. (a) Hypodermis of the whole thigh. Hypodermis appears hyperintense. The dermis is not visible at this spatial resolution; (b) High spatial resolution 2D image, 3 mm thick, of hypodermis on the dorsal side of the thigh of a woman with cellulite. With a resolution of 70 μm in depth of the skin, Camper's fascia separates the adipose tissue in two layers. Deep adipose indentations into the dermis are clearly visualized. Fibrous septae appear as hypointense thin structures. (c) Two contiguous thin images from a series of 64 images. A slice thickness of 0.5 mm offers an optimal contrast between fat lobules and fibrous septae allowing the 3D reconstruction of the fibrous network architecture.

with a classical spin echo sequence ($T_R = 1$ s, $T_E = 30$ ms, $T_{acq} = 2$min.) visualization of fibrous septae as hyposignal structures allowed the operator to determine graphically a volume of interest (VOI) of typically $2 \times 5 \times 6\,mm^3$ within a fat lobule (Fig. 2). A control image of the VOI was obtained with a stimulated echo acquisition method ($T_R = 500$ ms, mixing time (T_M) = 13.7 ms, $T_E = 30$ (ms) in order to check the absence of signals outside the selected VOI. Finally localized proton spectra were recorded (Fig. 2).

After manual shimming, a series of water-unsuppressed spectra ($T_R = 1520$ ms, 2500 Hz spectral width and 2048 data points) was thus acquired with the same sequence only varying T_M ($T_M = 13.7$, 45, 100, 200, and 500 ms) for T_1 measurement, and only varying T_E ($T_E = 30$, 40, 50, 75, 100, and 150 ms) for T_2 measurement.

Image processing

The thickness of the superficial and deep adipose layers was measured with WIMA software (*CNRS-UMR 7623, Paris, France*). 3D series were processed with matlab language (*The Mathworks, Natick, USA*), and dedicated 3D image processing algorithms developed with Tivoli routines (*ENST-TSI, Paris, France*). Finally 3D reconstructions were visualized on a workstation equipped with 3D Voxtool software (*General Electric, Milwaukee, USA*).

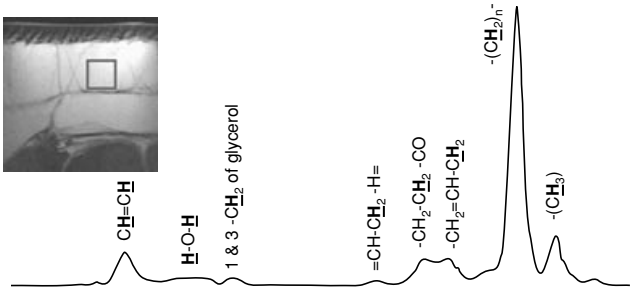

Fig. 2. In vivo proton MR spectrum in a fat lobule. Water resonance as well as 8 different lipid resonances are clearly resolved. The volume of interest is graphically selected by the operator within a fat lobule in order to avoid water-rich structures such as fibrous septae.

Spectra analysis

Spectra were first processed with SAGE/IDL software (*General Electric, Milwaukee, USA*) by applying an exponential filter, which produced a line broadening of 5 Hz, by zero filling to 4096 data points, and manual phasing after Fourier transform. No baseline correction was used. Then, T_1 and T_2 values were computed by fitting signal amplitudes according to relation 1:

$$S = \sum_i kN^i(H) e^{-\frac{T_M}{T_1^i}} e^{-\frac{T_E}{T_2^i}} \quad (1)$$

where $T_1{}^i$ and $T_2{}^i$ are relaxation times of resonance i, $N^i(H)$ is a function of the mobile proton density, and k, a function of the instrument's receiver gain.

Water content and the different lipid fractions were estimated using the advanced time domain signal-processing package MRUI (*MRUI V96.3, EU Network program: CHRX-CT94-0432*).

Statistics

Data were analysed with SPSS statistical software (SPSS, Chicago, USA). All results were expressed as mean ± standard deviation. Sex was studied by ANOVA between normal women and men. Cellulite-related effects were evaluated by comparing women with cellulite to women with no cellulite. *P*-values < 0.05 were considered to be significant.

Results

Anatomical characterization of SAT

Table 1 shows the thickness values of the skin and adipose layers. Women with cellulite are characterized by a thicker dermis compared to normal women ($P < 0.01$), but no sex-related effects have been observed. Women with cellulite have

TABLE 1. Mean values of skin and adipose layer thickness according to sex and presence of cellulite

	Dermal thickness (mm)	Subcutaneous adipose tissue thickness (mm)		
		Superficial layer	Deep layer	Total
Women with cellulite ($n = 21$)	1.87 ± 0.39[a]	8.41 ± 1.61	24.81 ± 4.90	34.02 ± 5.42
Women without cellulite ($n = 20$)	1.58 ± 0.21	4.03 ± 1.26	4.31 ± 1.82	8.34 ± 2.44
Men ($n = 23$)	1.71 ± 0.24	2.77 ± 1.63	3.87 ± 1.70	6.64 ± 3.16

[a]Standard deviation

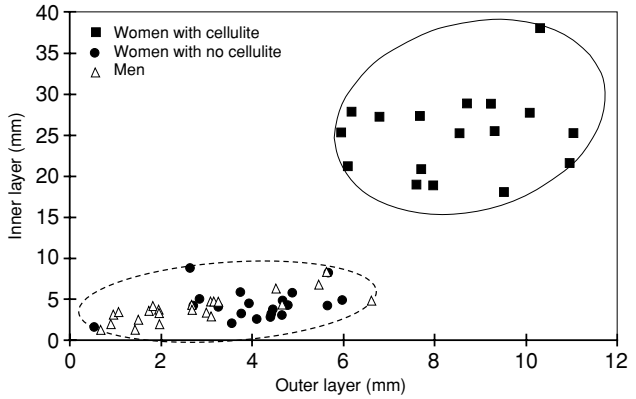

Fig. 3. New characteristic marker of cellulite. MR imaging shows that women with cellulite have a much greater increase in the thickness of the deep inner adipose layer compared to normal women or men.

thickened adipose layers compared to normal women or men ($P = 0.0001$).

Furthermore, the increase is much greater in the inner adipose layer than the superficial layer for women with cellulite (Fig. 3).

3D SAT anatomy was obtained after image processing of the 3D MR images. Figure 4 shows the 3D topography of the interface between dermis and adipose tissue for one subject of the three groups after semiautomatic image processing segmentation of the skin and the two different adipose layers. The mean height of adipose indentations into dermis are quantified by calculating an index of irregularity, R_T according to relation 2:

$$R_T = \frac{\text{Surf}_{\text{Dermo-hypodermal junction}}}{\text{Surf}_{\text{Refrence\_plane}}} \times 100 \qquad (2)$$

where $\text{Surf}_{\text{Dermo-hypodermal}}$ junction represents the number of pixels of the dermo–hypodermal interface, and $\text{Surf}_{\text{Reference\_plane}}$ the number of pixels of the scanned plane.

For the three groups, R_T mean values are presented in Table 2. It is significantly higher for women with cellulite ($P < 0.05$).

The second step aimed at describing the 3D architecture of the fibrous septae within the subcutaneous tissue. Figure 5 shows typical images for individuals of the 3 groups. After segmentation, only fibrous septae are visualized. Camper's fascia is clearly seen as a thin plane structure more or less parallel to the skin surface. Other septae were detected as thin pillar-like structures, and three principal orientations were calculated: perpendicular, parallel to the skin surface, and tilted at about 45° (Fig. 6). Women with cellulite have a higher percentage of perpendicular fibrous septae than normal women ($P < 0.001$) or men ($P < 0.01$). For the other two directions, according to presence of cellulite, women with cellulite are characterized by a smaller percentage of septae parallel to the skin ($P < 0.001$) and a higher percentage at 45° ($P < 0.001$). According to sex, there are no differences in these 2 directions.

Physiological characterization of SAT

Mean T_1 and T_2 values within a fat lobule, calculated from ^{1}H spectra, are listed in Table 3. None of these intrinsic physiological parameters of the adipose tissue are significantly different according to sex and presence of cellulite (Fig. 7).

Finally, we calculated, for the three groups the total fraction of saturated lipids (85.3 ± 5.9), unsaturated lipids (3.7 ± 2.3), and water (4.7 ± 5.6). There was no difference between the 3 groups, except according to sex there was a slight increase ($P < 0.05$) in unsaturated lipid fraction for normal women.

Discussion

Magnetic Resonance characterization of living tissues can be obtained not only from anatomic cross-section images but also by determining intrinsic MR parameters such as T_1 and T_2 relaxation times and proton density, as well as performing

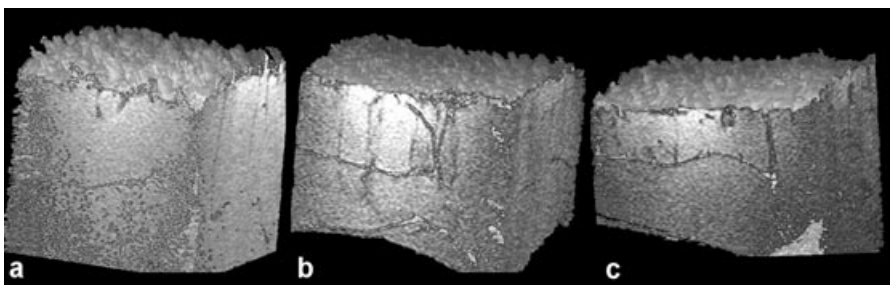

Fig. 4. Visualization of the 3D topography at the interface between dermis and subcutaneous tissue. (a) Woman with cellulite; (b) Normal woman; (c) Man. Deep adipose indentations into the dermis are a characteristic marker of cellulite.

TABLE 2. Mean values of the index of irregularity of the 3D topography at the dermo–hypodermal interface according to sex and presence of cellulite. This index quantifies the mean height of adipose indentations into dermis (A.U. Arbitrary units)

	Index of irregularity (A.U)
Women with cellulite ($n = 16$)	2.29 ± 0.32[a]
Women without cellulite ($n = 17$)	2.08 ± 0.12
Men ($n = 20$)	1.91 ± 0.24

[a]Standard deviation

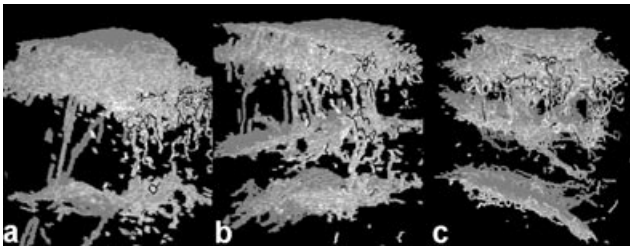

Fig. 5. Visualization of the 3D architecture of fibrous septae in subcutaneous adipose tissue. (a) Woman with cellulite; (b) Normal woman; c: Man.

localized spectroscopy in order to yield quantitative information about various metabolites.

Anatomical characterization of SAT

Magnetic Resonance imaging is a very efficient tool for measuring not only the thickness of skin and hypodermis but also the surface and volume of hypodermis. Our results confirmed an increase in skin thickness (unpublished data obtained with high frequency ultrasound) in women with cellulite, as well as the presence of deep indentations of adipose tissue into the skin as previously shown by high frequency ultrasound (26, 27), and by histology (23). High spatial resolution MR imaging enabled us to detect for the first time Camper's fascia, formerly demonstrated by histology (31), as well as to measure independently the superficial and deep adipose layers within the hypodermis. A thicker deep adipose layer is a notable marker of cellulite.

The 3D architecture of fibrous septae revealed that Camper's fascia was a thin plane structure 'parallel' to the skin surface. Vertical septae appeared as pillar-like structures in contradiction with straight planes proposed on diagrams by Nürnberger et al. On a first hand, histological pictures from planes parallel to the skin surface (unpublished personal data) revealed thin fibrous septae of 30–70 μm in thickness. On a second hand, a recent upgrading of the gradient coils of our MR imaging system, allowed us to acquire, for

TABLE 3. Mean values of the relaxation times T_1 and T_2 of lipids and water in adipose tissue

Metabolite	T_1 (ms)	T_2 (ms)
Lipid1: CH = CH	290 ± 55[a]	47 ± 7
Lipid2: 1- & 3-CH_2-glyc	164 ± 25	30 ± 10
Lipid3: = CH-CH_2-H =	272 ± 60	49 ± 15
Lipid4: -CH_2-CH_2-CO	169 ± 35	50 ± 12
Lipid5: -CH_2 = CH-CH_2-	213 ± 35	46 ± 17
Lipid6: -$(CH_2)_n$-	219 ± 30	82 ± 11
Lipid7: -CH_3	366 ± 71	92 ± 30
Water: H-O-H	169 ± 61	30 ± 9

[a]Standard deviation calculated from 62 subjects

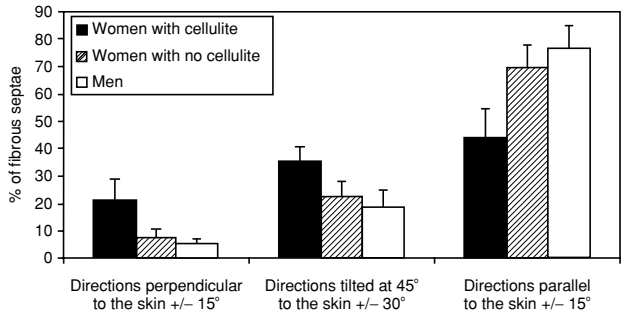

Fig. 6. Structured patterns of the fibrous septae network according to sex and presence of cellulite. Our quantitative findings gives more evidence about the heterogeneity in the directions of the septae, and highly suggest that modelizing the 3D architecture of fibrous septae as a perpendicular pattern in women whereas tilted at 45° in men would be an over simplification.

the first time, high spatial resolution MR images of the subcutaneous adipose tissue of an *ex vivo* sample, in a plane parallel to the skin surface. Figure 8 (FOV = $20 \times 20\,mm^2$, resolution: $78 \times 78\,\mu m^2$, slice thickness = 300 μm) clearly depicts a more randomly organized pattern of the fibrous network along with the presence of localized thickened septae. This probably corresponds to the detected structures on 3D images. Although fine details of the network remain undetected, our findings, however, allow quantification of the main directions of this fibrous network. For women with cellulite, we found a higher percentage of septae perpendicular to the skin surface and a smaller percentage parallel to the surface. In some aspects, our results are in agreement with those of Nürnberger, but this present work gives more evidence about the heterogeneity in the directions of the septae. These findings highly suggest that modelizing the 3D architecture of the fibrous septae network as a perpendicular pattern in women whereas criss-cross in men would be an over simplification.

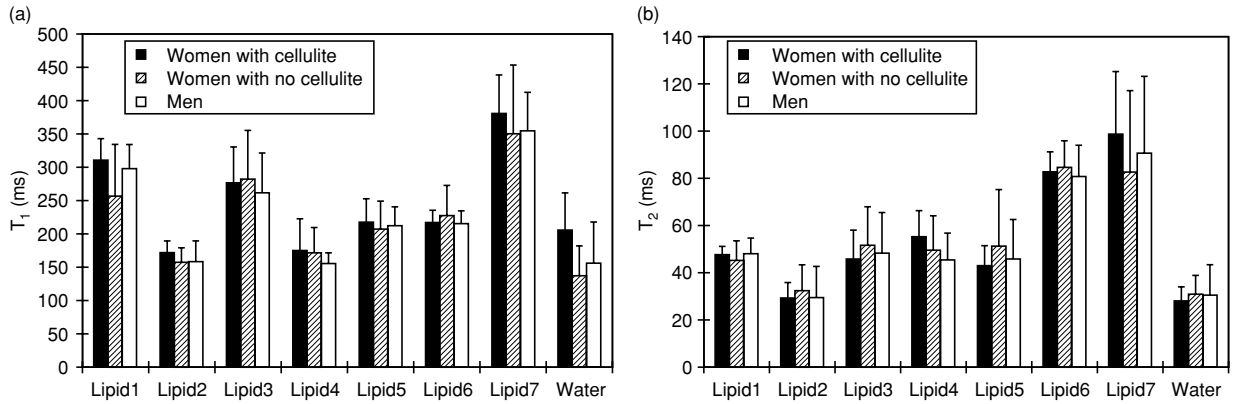

Fig. 7. Mean values of the relaxation times T_1 and T_2 of lipids and water in adipose tissue according to sex and presence of cellulite. There are no differences among all the subjects.

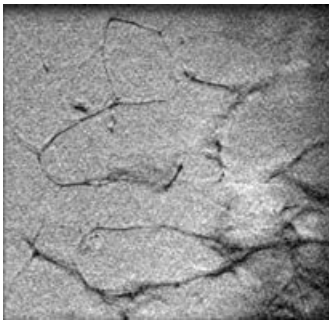

Fig. 8. High spatial resolution (voxel size = $78 \times 78 \times 300$ μm^3) 2D MR image of the fibrous septae network in a plane parallel to the skin surface. The thin tortuous hypointense structures represent fibrous septae. Thickened areas are visible and probably correspond to those visible on the 3D reconstructions.

Physiological characterization of SAT

Changes in the physiology of the subcutaneous tissue in relation to sex and presence of cellulite are still a matter of controversy. We first evaluated relaxation times of the different chemical compounds detected by proton spectroscopy, which reflect the dynamic aspect of biologic systems. T_1 and T_2 values of lipid compounds were consistent with those previously reported (16). The measurement of short T_1 and T_2 values for water showed that the content was low along with a restricted motion. No difference according to sex or cellulite was found. Data for the unsaturated lipid fraction, saturated lipid fraction, and water fraction were similar for the three groups, except for a slight inexplicable increase in the unsaturated lipid fraction for normal women compared to men. There have been reports that some differences had been measured according to dietary restrictions (32), and body sites (33), but our findings are in good agreement with other studies where there were no differences in saturated and unsaturated fatty acids in normal adipose tissue (27, 33). For our 67 subjects regardless of sex and presence of cellulite, subcutaneous adipose tissue contains about 7.4% of water, and 92.6% of lipids distributed as 7.3% of unsaturated lipids and 85.3% of saturated lipids.

Our MR findings did not confirm the hypothesis of an increase in water content of subcutaneous adipose tissue in case of cellulite as suggested by some authors (28), except if excess water was located in the connective septae as our measurements were strictly limited within a fat lobule. Unfortunately, this hypothesis should be extremly difficult to confirm by an MR study as *in vivo* MR spectroscopy has not enough sensitivity to acquire a localized spectrum within a single connective septum.

In conclusion, high resolution MR imaging and localized spectroscopy allowed us to go a step further in the knowledge of *in vivo* subcutaneous adipose tissue anatomy and physiology. Our results on healthy subjects can serve as reference data for the characterization of diseased conditions as well as sub-clinical alterations of adipose tissue. Concerning the specificity of cellulite, MR imaging revealed some modifications of adipose tissue anatomy, but MR spectroscopy did not detect any physiological modification.

Acknowledgements

The authors wish to thank Dr J.L. Lévêque (L'Oréal-Recherche, Clichy, France) for fruitful discussion, and Professor A.M. Kligman (University of Pennsylvania, Philadelphia, USA) for critical reading of the manuscript.

References

1. Kissebah AH, Peiris AN. Biology of regional body fat distribution. Relationship to non-insulin-dependent diabetes mellitus. Diabetes Metab Rev 1989; 4: 615–622.
2. Björntorp P. Adipose tissue distribution and function. Int J Obesity 1991; 15: 67–81.
3. Hayes PA, Sowood PJ, Belyavin A, Cohen JB, Smith FW. Sub-cutaneous fat thickness measured by magnetic resonance imaging, ultrasound, and calipers. Med Sci Sport Exercise 1988; 20: 303–309.
4. Arner P, Kriegholm E, Engfeldt P. In situ studies of catecholamine-induced lipolysis in human adipose tissue using microdialysis. J Pharmacol Exp Ther 1990; 15: 254–284.
5. McNeill G, Fowler PA, Maughan RJ, McGaw BA, Fuller MF, Gvozdanovic D, Gvozdanovic S. Body fat in lean and overweight women estimated by six methods. Br J Nutr 1991; 65: 95–103.
6. Ross R, Shaw KD, Rissanen J, Martel Y, De Guise J, Avruch L. Sex differences in lean and adipose tissue distribution by magnetic resonance imaging: anthropometric relationships. Am J Clin Nutr 1994; 59: 1277–1285.
7. Thomas EL, Saeed N, Hajnal JV, Brynes A, Goldstone AP, Frost G, Bell JD. Magnetic resonance imaging of total body fat. J Appl Physiol 1998; 85: 1778–1785.
8. Fowler PA, Fuller MF, Glasbey CA, Foster MA, Cameron GG, McNeill G, Maughan RJ. Total and subcutaneous adipose tissue in women: the measurement of distribution and accurate prediction of quantity by using magnetic resonance imaging. Am J Clin Nutr 1991; 54: 18–25.
9. Marks SJ, Chin S, Strauss BJG. The metabolic effects of preferential reduction of visceral adipose tissue in abdominally obese men. Int J Obesity 1998; 22: 893–898.
10. Dooms GC, Hricak H, Sollito RA, Higgins CB. Lipomatous tumors and tumors with fatty component. MR imaging potential and comparison of MR and CT results. Radiology 1985; 157: 479–483.
11. Saiag P, Le Breton C, Pavlovic M, Fouchard N, Delzant G, Bigot JM. Magnetic resonance imaging in adults presenting with severe acute infectious cellulitis. Arch Dermatol 1994; 130: 1150–1158.
12. Idy-Peretti I, Bittoun J, Alliot FA, Richard S, Querleux B, Cluzan RV. Lymphedematous skin and subcutis: *in vivo* high-resolution magnetic resonance imaging evaluation. J Invest Dermatol 1998; 110: 101–106.
13. Olhager E, Thuomas KA, Wigstrom L, Forsum E. Description and evaluation of a method based on magnetic resonance imaging to estimate adipose tissue Volume and total body fat in infants. Pediat Res 1998; 44: 572–577.
14. Liang MD, Narayanan K, Davis PL, Futrell JW. Evaluation of facial fat distribution using magnetic resonance imaging. Aesth Plast Surg 1991; 15: 313–319.
15. Bittoun J, Querleux B. Visualisation et caractérisation de la graisse sous-cutanée en imagerie par résonance magnétique (IRM) à haute résolution spatiale. In. *Vaisseux et tissu adipeux* (Cluzan RV, Alliot FA, Ascher B., eds). Lavaur: Editions médicales Pierre Fabre 1997; 65–73.
16. Schick F, Eismann B, Jung WI, Bongers H, Bunse M, Lutz O. Comparison of localized proton NMR signals of skeletal muscle and fat tissue in vivo: two lipid compartments in muscle tissue. Magn Reson Med 1993; 29: 158–167.
17. Dzendrowskyj TE, Noyszewski EA, Beers J, Bolinger L. Lipid composition changes in normal breast throughout the menstrual cycle. Magma 1997; 5: 105–110.
18. Querleux B, Jolivet O, Bittoun J. In vivo proton magnetic resonance spectroscopy in human skin. In: Current Problems in Dermatology Vol. 26 (Elsner, P, Barel, AO, Berardesca, E, Gabard, B, Serup, J, eds). Karger 1998; 12–19.
19. Thomas EL, Cunnane SC, Bell JD. Critical assessment of in vivo C-13 NMR spectroscopy and gas-liquid chromatography in the study of adipose tissue composition. NMR Biomed 1998; 11: 290–296.
20. Lunati E, Marzola P, Nicolato E, Fedrigo M, Villa M, Sbarbati A. In vivo quantitative lipidic map of brown adipose tissue by chemical shift imaging at 4.7 tesla. J Lipid Res 1999; 40: 1395–1400.
21. Thomsen C, Becker U, Winkler K, Christoffersen P, Jensen M, Henriksen O. Quantification of liver fat using magnetic resonance spectroscopy. Magn Reson Imaging 1994; 12: 487–495.
22. Millis KK, Maas WE, Cory DG, Singer S. Gradient, high-resolution, magic-angle spinning nuclear magnetic resonance spectroscopy of human adipocyte tissue. Magn Reson Med 1997; 38: 399–403.
23. Nurnberger F, Muller G. So-called cellulite: an invented disease. J Dermatol Surg Oncol 1978; 4: 221–229.
24. Pierard GE, Nizet JL, Pierard-Franchimont C. Cellulite: From standing fat herniation to hypodermal stretch marks. Am J Dermatopathol 2000; 22: 34–37.
25. Querleux B. Characterization of the human skin in vivo: high frequency ultrasound imaging and high spatial resolution magnetic resonance imaging. Euroson 98, Tours, France, March 26–30, 1998 (book of Abstract).
26. Lucassen GW, van der Sluys WLN, van Herk JJ, Nuijs AM, Wierenga PE, Barel AO, Lambrecht R. The effectiveness of massage treatment on cellulite as monitored by ultrasound imaging. Skin Res Technol 1997; 3: 154–160.
27. Rosenbaum M, Prieto V, Hellmer J, Boschmann M, Krueger J, Leibel RL, Ship AG. An exploratory investigation of the morphology and biochemistry of cellulite. Plast Reconstr Surg 1998; 101: 1934–1939.
28. Ryan TJ, Curri SB. Blood vessels and lymphatics. Clin Dermatol 1989; 7: 25–36.
29. Scherwitz C, Braun-Falco O. So-called cellulite. J Dermatol Surg Oncol 1978; 4: 230–234.
30. Bittoun J, Saint-Jalmes H, Querleux B, Jolivet O, Darrasse L, Idy-Peretti I, Leroy-Willig A, Lévêque JL. In vivo high-resolution MR imaging of the skin in a whole-body system at 1. 5T Radiology 1990; 176: 457–460.
31. Markman B. Anatomy and physiology of adipose tissue. Clin Plast Surg 1989; 16: 235–244.
32. Bailey JW, Walker E, Beauchene RE. Fatty acid composition of adipose tissue in aged rats. Effects of dietary restriction and exercise. Exp Gerontol 1993; 28: 233–247.
33. Pittet PG, Halliday D, Bateman PE. Sites differences in the fatty acid composition of subcutaneous adipose tissue of obese women. Br J Nutr 1979; 42: 56–61.

Address:
Dr Bernard QUERLEUX
L'Oréal-Advanced Research Laboratories
1, avenue Eugène SCHUELLER
93601 Aulnay-sous-bois
France

Tel: 33 148 68 96 41
Fax: 33 148 68 99 24
e-mail: bquerleux@recherche.loreal.com